

DETERMINATION OF STATIC FLOW CHARACTERISTICS OF A PROTOTYPICAL DIFFERENTIAL VALVE USING COMPUTATIONAL FLUID DYNAMICS

Marcin KISIEL*^{ORCID}, Dariusz SZPICA*^{ORCID}

*Faculty of Mechanical Engineering, Białystok University of Technology, Wiejska 45C, 15-351 Białystok, Poland

marcin.kisiel@sd.pb.edu.pl, d.szpica@pb.edu.pl

received 21 November 2023, revised 18 May 2024, accepted 20 May 2024

Abstract: The paper describes the numerical calculations of a conceptual air brake valve of a trailer equipped with a differential section, which is intended to shorten response time and braking distance. The static flow characteristics have been determined using computational fluid dynamics (CFD). Mixed (global and local) computational meshes were used in the paper to determine the static flow characteristics of the valve sections. The use of the local mesh was relevant for valve openings smaller than 0.5mm. Using CFD, it was possible to determine the static flow characteristics of the main, auxiliary feed and the differential sections, which were linear, degressive and progressive depending on the section. The analyzes, which have not yet been described in the literature, showed a significant difference in the MFR of the additional and main feed tracts, which reached 52.29%. The results are applicable to the configuration of the braking system. Further research will include performing dynamic simulations using dedicated software and building a test rig to validate the CFD calculation results.

Key words: Mechanical engineering, differential braking valve, pneumatic braking valve, CFD, static flow characteristics

1. INTRODUCTION

Technological developments in agriculture [1][2], particularly organic farming [3]-[5], have encouraged the increasing use of air and hydraulic braking systems widely used in crop trailers. What works in favour of pneumatic systems is the lack of possibility of environmental and groundwater contamination [6] in the event of damage. Maintaining the agricultural tractor, machinery and trailers in good working order contributes to reducing the possibility of environmental pollution. Replacement of pneumatic solutions for trailer braking systems used in agriculture with hydraulic solutions has made it possible to improve the performance of the system with a concomitant increase in the risk of environmental pollution from hydraulic oil [7]. Environmental pollution can occur during coupling, uncoupling of the trailer or in the event of a system failure, while the use of a pneumatic braking system neutralizes this risk, limiting it to the emission of only the products of wear of the friction material of the brake linings [8][9] used in transport trailers.

Pneumatic braking systems are widely used in the transportation industry, both on truck tractors and agricultural tractors, as well as semi-trailers and trailers. Due to the increasing normative requirements [10] imposed by regulations, classical systems controlled by pneumatic signals are gradually being replaced by hydraulic systems and electropneumatic solutions [11]. This is due to the much faster response time of the above systems compared to fully pneumatic systems [12]. The authors noted the possibility of introducing design changes, in one of the most widely used classic valves for activating the brakes of a trailer Visteon 44100110, also called HZS-02 valve, introducing a differential (accelerating) section. On the basis of preliminary analyses [13], it was noted that the response time of the system was significantly

reduced compared to the original solution, and the performance of hydraulic and electro-pneumatic systems was brought closer [14].

Computational fluid dynamics (CFD) is finding increasing application in various industries due to its capabilities and reliable results. The results of CFD numerical calculations are obtained by solving a system of differential equations describing the flow of a gas or liquid in a simulated system [15]. Numerical modeling using CFD provides an alternative approach to determining flow parameters such as velocity, pressure, flow type and temperature at any point in a concentrated volume with respect to complex and elaborate analytical models. CFD methods use the Reynolds-Averaged Navier-Stokes (RANS) equations [16][17] to search for a solution and allow evaluation of the effect of changing the model boundary conditions on the static characteristics of the valve without the need for verification on a laboratory bench. Determining the pressure in the concentrated volume and the MFR (Mass Flow Rate) or VFR (Volumetric Flow Rate) gives the possibility to determine the static characteristics of the valve depending on its degree of opening and varying boundary conditions. The solution of the stream flow equations by local resistances, which are structural elements of the geometry under consideration, allow determining the velocity and pressure in any section of the simulation model. Numerical methods are used to determine flow parameters [18][19] and static characteristics [20] necessary for the correct selection of pneumatic and hydraulic components, including valves [21]-[24].

The high level of accuracy and quality of the simulation results obtained is largely dependent on the degree of discretization of the model resulting from the computational mesh used [25][26]. Over-densification of the global mesh in the clustered volume does not significantly improve the obtained results, but increases the simulation time [27][28]. In order to densify the model in sensitive areas (narrow gaps), SolidWorks uses additional tools like

channels and equidistant refinement, that create a local mesh in the declared area bounded by the model planes. Other CFD tools, including Ansys Fluent, allow changing the shapes of computational mesh elements and creating hybrid meshes that form a combination of two or more default mesh types.

Attempts at numerical modeling of pneumatic brake valves [29]-[31] have been noted among numerous research papers. The authors recognized a research gap related to the lack of studies containing attempts to simulate models of pneumatic brake valves as whole actuating components, using computational fluid mechanics (CFD) tools.

Pneumatic systems, although increasingly displaced by hydraulic systems, do not pose an environmental hazard in the event of a system leak. Despite the longer response time of the pneumatic system compared to the hydraulic system in agricultural transport, the most common are combination systems that allow connection with the air or hydraulic braking system of the tractor.

The following sections of the article present the structure of the research object, the proposal of design changes introducing the differentiation term proposed by the authors, the theoretical basis for the numerical solution of flow problems and the boundary conditions of the performed numerical analyses. Mesh convergence assessment enabled the selection of appropriate settings for a given geometry while maintaining optimal simulation time. Based on the selected mesh settings, CFD simulations were performed for three sections of the considered valve, taking into account different degrees of opening or diameter of the flow channel, taking into account the simplifications required for the correct implementation of the model in the CFD environment. The determined MFR values made it possible to determine the static flow characteristics of the trailer's pneumatic brake valve in its various power supply sections, which constitutes a research gap and is an introduction to the analysis of the results obtained using numerical and experimental methods, which are the authors' research area. The proposed modification of the structure of the trailer brake valve will shorten the response of the braking system in emergency braking situations and will probably lead to its implementation in industry, after additional numerical and experimental tests.

2. OBJECT OF RESEARCH

2.1. Trailer air brake valve Visteon 44100110

For the implementation of the prototype differential valve, the Visteon 44100110 trailer brake valve was used (Fig. 1).



Fig. 1. Visteon 44100110 trailer brake valve

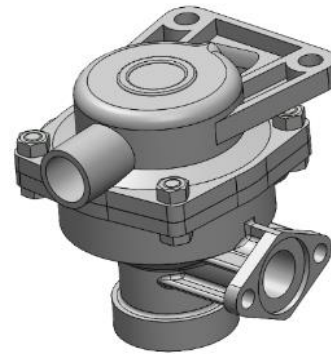


Fig. 2. CAD model of Visteon 44100110 brake valve

Fig. 1 shows a view of the original valve, while Fig. 2 shows a CAD model of the valve created in SolidWorks software. The selected valve can work with both single- and dual-line systems, and a description of the valve's connection to both types of tractor air brake systems is shown in Tab. 1.

Tab.1. Description of valve connections

Symbol	M	Zm	V	Z
Single line system	Connected with brake supply and control section	Not connected and sealed	Connected with compressed air reservoir of a trailer	Connected directly into brake actuator or brake force regulator
Dual line system	Connected with brake supply section	Connected with brake control section		

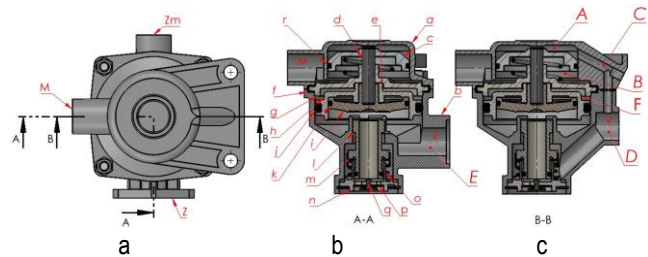


Fig. 3. View of the valve: a - top view; b - A-A cross-sectional view of main supply line; c - B-B cross-sectional view of additional supply line

Based on the valve construction diagram Fig. 3, it should be noted that during single-line operation, the pneumatic control and supply signal from the *M* connection, feeds the compressed air tank chamber of the trailer *D* by flowing between the surface of the piston *c* with lip seal *r* and the valve body *a* and further through channel *C*. During driving, the valve performs the function of supplying the reservoir, and the chamber *E* is vented through the vent *p* due to the passage between the seat in the piston *i* and the bushing *l*. Applying the brakes causes a pressure drop in the *M* connection and chamber *A*, which translates into a pressure difference between the reservoir connection *V* and the supply and control connection *M*. The pressure difference causes the chamber over the piston *c* to seal, overcoming the tension force of the spring *e* and displacing the piston *c* together with the guide *d* and piston *i* to the bushing *l* closing the connection with the atmosphere and opening the passage between the bushing *l* and the

body *b* from the tank chamber *D* to the chamber *E* connected with brake actuator. The increasing pressure in the chamber under the piston *i* and the force of the tension of the spring *o* causes the gradual movement of the piston assembly and bushing *l* until the connection between the output connection *Z* and the chamber of the tank *D* is closed. Depending on the ratio of pressures above and below the piston *i*, the braking force is reduced, causing the trailer to be decelerated and the air cylinders to be vented through the vent *p*.

Connection of the valve in a two-line system requires the use of a control port *Zm* connected to the control chamber *F* under the element *g*. When the brakes are applied, the increasing pressure in the *Zm* connection causes the displacement of pistons *h* and *i* down into bushing *l* and the closing of the connection of chamber *E* with atmospheric pressure through vent *p*. The downward displacement of bushing *l*, after overcoming the force in spring *o*, causes the connection of chambers *D* and *E* and the application of the trailer brakes. The pressure drop in the *Zm* connection caused by the deceleration of the vehicle combination causes the displacement of pistons *h* and *i* and the opening of the passage between piston *i* and bushing *l*, while closing the connection of chambers *D* and *E*. When the valve is switched to the reservoir supply function, the chambers of the pneumatic cylinders are vented through the vent *p*, and the trailer brakes are released.

2.2. Conceptual differential braking valve

The conceptual differential valve was obtained by appropriate modifications to the base valve shown in Fig. 3. The modified valve is shown in Fig. 4. The main change was the replacement of the main supply connection with a tee *p*, which also supplies through the s-connector and *t*-wire a chamber *A* above piston *c*.

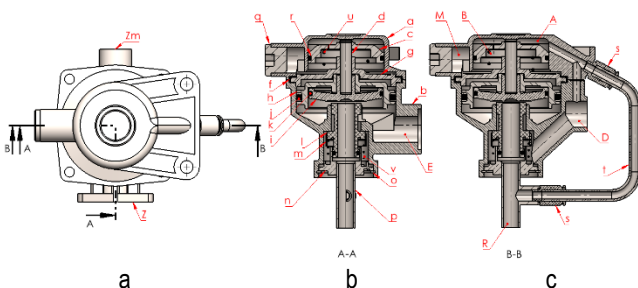


Fig. 4. View of differential valve; a - top view; b - A-A cross-sectional view of main supply tract; b - B-B cross-sectional view of differential tract

The existing supply connection *M* has been plugged with a plug *q*. At the same time, the valve is supplied by bushing *l* and the gap under piston *i* is adjusted by the position of piston *i* and bushing *l* regulates the supply of chamber *E* connected directly to the brake actuator. In the case of slow braking (Fig. 5), the tee *p* connection is supplied with compressed air and further supplies the output connection. The differential section in this case remains inactive, due to the small pressure difference between chambers *A* and *B*.

In the case of panic braking (Fig. 6), there is a rapid pressure increase in the chamber *A*. The nozzle used with the appropriate cross-section restricts the flow between chambers. The increasing pressure in chamber *A* causes the valve's differential section to operate and move the piston *c* together with the pin *d* and the pistons *h*, *i* toward bushing *l* and close the supply from the tee *p*.

The movement of the pistons and resting on the wall of bushing *l* causes it to move downward and open the supply to chamber *E* from an additional compressed air reservoir (chamber *D*) located near the valve.

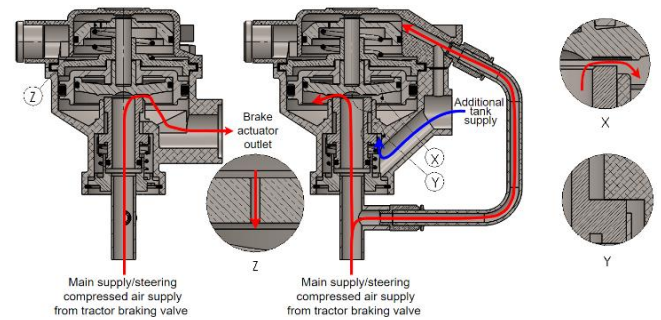


Fig. 5. Slow braking

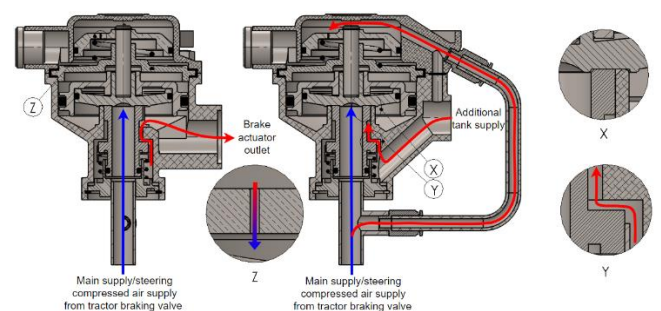


Fig. 6. Emergency, rapid braking

In the situation of equalization of pressures in chambers *A* and *B* (Fig. 7) there is an upward displacement of pistons *c*, *h*, *i* with the pin *d* caused by the force in the spring *u*. This action causes deactivation of differential section and closure of the valve supply from the additional air reservoir and transition to the tracking action resulting from the valve supply from the tee *p*.

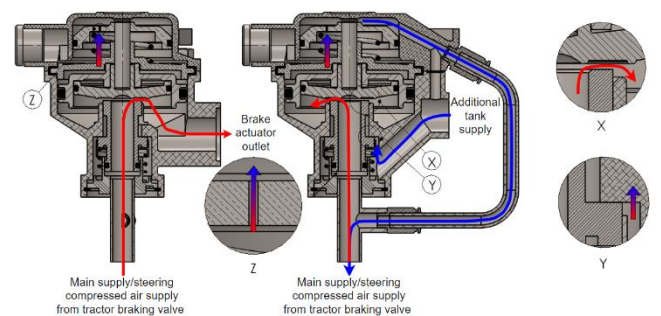


Fig. 7. Switching the braking valve to tracking function

3. CALCULATION METHODOLOGY

3.1. Theoretical basis

The preponderance of flow calculation software uses the Finite Volume Method (FVM) [32][33]. This method is based on the division of extended geometries into smaller volumes, in which it is possible to determine the distributions of characteristic quantities, mainly flow velocity, pressure, density, temperature and others, without having to search for a general solution for the entire model. The division of concentrated volumes into individual

cells makes it possible to determine the values of its flow parameters on the basis of the balance of a given cell and neighboring cells.

The SolidWorks Flow Simulation used in this study uses an orthogonal mesh of concentrated volumes based on orthogonal cells with walls parallel to the planes of the model's main coordinate system. The computational mesh, depending on the declared settings, can be the same size throughout the model cross-section (global mesh) or thicken in sensitive areas with a limited flow field (local mesh). By default, the mesh tools available in SolidWorks Flow Simulation allow the definition of seven degrees of global mesh density. The quality of the clustered volume mesh has a key impact on accuracy and calculation time, so local global mesh densities are used to minimize model discretization errors. However, the final mesh selection should be preceded by an assessment of mesh convergence for a given geometry. Local mesh options include additional tools such as equidistant refinement and channels. Equidistant refinement allows a 9-degree thickening of the liquid or working gas area within a normal distance from the selected model element. Channels allows the mesh to be compacted into narrow channels bounded by the model walls to obtain the best flow velocity distribution profile.

The finite volume method, which is the basis of CFD numerical calculations, including SolidWorks Flow Simulation, is based on dividing a continuous flow area into a set of discrete cells of a certain volume depending on the grid size, and determining by numerical methods the flow parameters of a liquid or gas stream by obtaining the solution of a system of differential equations. The search for a solution is limited to the principle of conservation of momentum for a moving gas according to the conservation of mass (1) [34] and the Navier-Stokes equations (2) [35]. The solution of these equations makes it possible to determine the velocity and pressure in any section of the model for any geometry.

$$\frac{\partial p}{\partial t} + \nabla(pv) = 0 \quad (1)$$

$$p \frac{\partial v}{\partial t} = -\nabla p + \rho g + \mu \nabla^2 v \quad (2)$$

SolidWorks Flow Simulation allows simulation of laminar as well as turbulent flows, with the Navier-Stokes equations with Favre mass averaging [36][37] being used for turbulent flows of compressible gases. This type of calculation provides an opportunity to take into account the effect of turbulence on flow parameters using the $k-\varepsilon$ turbulence model, the solution of which is to find the value of μ_t shown in equations (3) and (4) based on the kinetic energy of the vortices k and the rate of dispersion ε .

$$\mu_t = \rho v_t = \rho C_\mu \frac{k^2}{\varepsilon} \quad (3)$$

$$C_\mu = \left(\frac{3C_k}{2}\right)^{-3} \cong 0.1 \quad (4)$$

where: ε – rate of dispersion, k – kinetic energy of vortices for RANS model, ρ – gas density, C_μ – constant ~ 0.1 , C_k – Kolomogorow constant, $C_k=1.4-1.5$, v_t - turbulent viscosity coefficient.

The components of equation (3) for the kinetic energy of turbulence are shown in equation (5), and for the energy of dispersion in (6):

$$\frac{\partial \rho k}{\partial t} + \frac{\partial \rho k v_i}{\partial x_i} = \frac{\partial}{\partial x_i} \left(\left(\mu + \frac{\mu_i}{\sigma_k} \right) \frac{\partial k}{\partial x_i} \right) + \tau_{ij}^R \frac{\partial v_i}{\partial x_j} - \rho \varepsilon + \mu_t P_B \quad (5)$$

$$\frac{\partial p k}{\partial t} + \frac{\partial \rho \varepsilon v_i}{\partial x_i} = \frac{\partial}{\partial x_i} \left(\left(\mu + \frac{\mu_i}{\sigma_k} \right) \frac{\partial k}{\partial x_i} \right) + C_{\varepsilon 1} \frac{\varepsilon}{k} \left(f_1 \tau_{ij}^R \frac{\partial v_i}{\partial x_j} + C_B \mu_t P_B \right) - f_2 C_{\varepsilon 2} \frac{\rho \varepsilon^2}{k} \quad (6)$$

where: $\sigma_{k,\varepsilon}$ - turbulent Prandtl number.

3.2. Calculation plan

The CFD numerical calculations included an assessment of the convergence of the global mesh for the geometry under consideration. Using all available mesh sizes in SolidWorks Flow Simulation, a simulation was carried out using constant boundary conditions in all variants to determine the effect of the mesh used on the values of the average relative and absolute error.

The second step involved determining the static characteristics of the main supply section of the prototype differential valve over the entire operating range (0...2.0) mm with a step of 0.1 mm. The defined boundary conditions made it possible to evaluate the effect of the degree of valve opening on the Mass Flow Rate (MFR) at the pneumatic actuator port Z (Fig. 4).

The third step involved the determination of the static characteristics of the additional accelerating tract in the situation of activating the differential section according to Section 2.2. The static characteristics were determined over the full operating range (0...1.7) mm with a step of 0.1 mm.

The last step of the calculation was to determine the static flow characteristics for the differential system with a nozzle of (0.75...3) mm in diameter in 0.25 mm increments placed in the piston c (for simplicity, the nozzle model was replaced by a hole) between chambers A and B of the simulation model.

Before determining the static characteristics of the conceptual valve, it was predicted that in the case of a slow build-up of pressure in the control connection, the pressure difference in the differential section (chambers A and B) will be negligibly small. In the case of sudden (panic) braking, a large difference in pressure between chambers A and B will cause activation of the differential section, closure of the control signal supply to the control-power connection and opening of the supply to the connection with an additional pressure reservoir located in a short distance from the valve, which will switch the valve to the acceleration function. Once the pressures in chambers A and B are equalized, the supply from the additional reservoir will be closed with a slight pressure surge due to the higher pressure value in the executive connection with respect to the supply and control connection.

4. RESULTS AND DISCUSSION

4.1. Assessment of the sensitivity of the computational mesh

As specified in the calculation plan, the sensitivity of the calculation grid was first evaluated. Based on the basic mesh sizes and fixed boundary conditions defined in SolidWorks Flow Simulation, the effect of the global mesh size on the MFR was investigated with the main valve feed section opening at the center of the operating range - 1.0 mm.

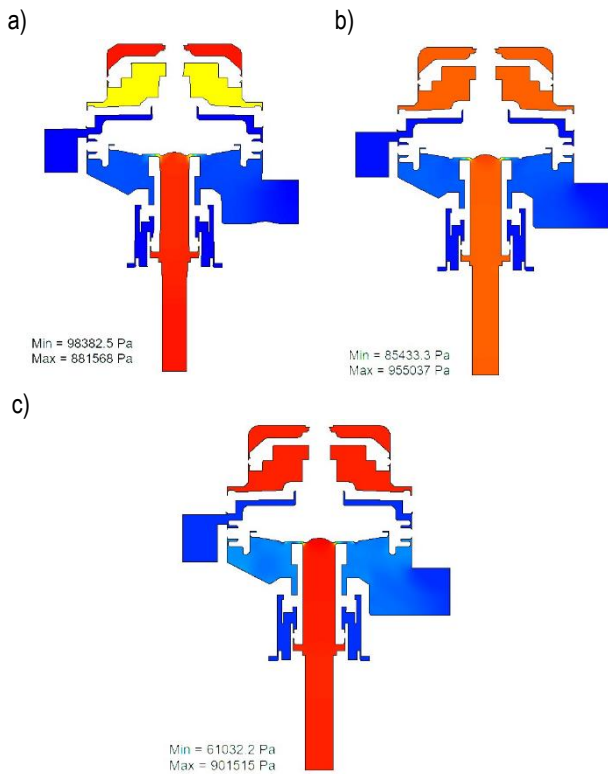


Fig. 8. Pressure distribution for different global mesh densities in SW Flow Simulation: a – first level; b – fourth level; c – seventh level

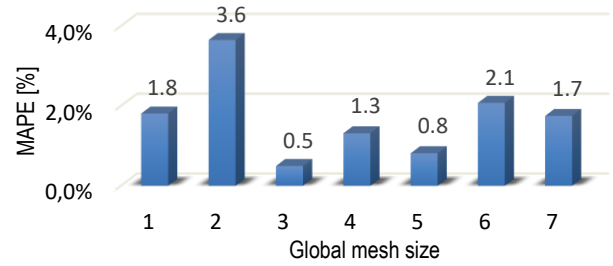


Fig. 9. MAPE value for different global mesh sizes

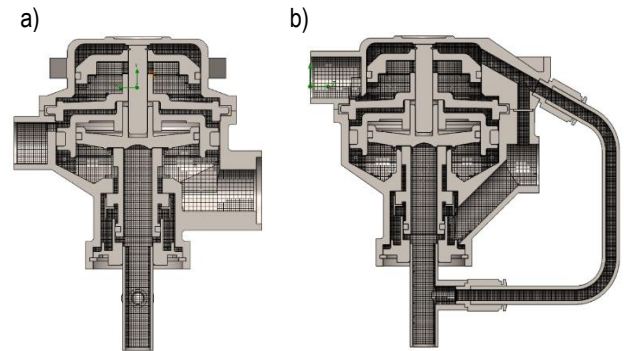


Fig. 10. Cross-sectional view of model with global mesh in 6th size: a - front plane view; b - right plane view

Tab. 2. Results of mesh convergence assessment

Mesh size	1	2	3	4	5
MFR [kg/s]	0.090821	0.089119	0.092036	0.093707	0.093245
Fluid cells	7209	4228	19449	45606	128290
Cells	6817	4076	14610	29170	65336
Iterations	46	45	104	132	150
Time [s]	15	11	45	105	251
MAE	0.001671	0.003374	0.000457	0.001215	0.000752
MAPE[%]	1.8%	3.6%	0.5%	1.3%	0.8%
Mesh size	6	7			
MFR [kg/s]	0.094412	0.094110			
Fluid cells	13295523	3512115			
Cells	44101	889461			
Iterations	259	365			
Time [s]	3678	13056			
MAE	0.001919	0.001617			
MAPE[%]	2.1%	1.7%			

Based on the results obtained, as shown in Tab. 2, it was concluded that a global mesh size of 3 or 5 should be adopted for further study, as they have the lowest MAPE (Mean Absolute Percentage Error) in the case under consideration. Careful observation of the distribution of the global mesh in both cases and solver errors reporting the occurrence of turbulence affecting the final results decided to exclude these two grid sizes from further study.

In order to reduce simulation time, authors decided to use the global mesh in 6th size with an additional local mesh with the channels and equidistant refinement tools in critical areas. Using a finer mesh would have significantly increased computation time.

4.2. Determining the static flow characteristics

Before the appropriate calculations in SolidWorks Flow Simulation, the model has been simplified to enable correct implementation in the numerical environment:

- the pressure value in the main supply port was replaced by a fixed value of 901325 Pa, in the other connections of the valve the value was set to 101325 Pa. In the case of the implementation of the simulation of the acceleration section, the value of 901325 Pa was declared in the connection of the additional compressed air tank, and the pressure in the main supply connection was replaced by the value of atmospheric pressure 101325 Pa,
- the springs *u*, *v* were removed (Fig. 4),
- all o-ring seals were replaced with square seals,
- The circlips were removed and replaced with ring elements (the circlips caused leaks in the model).

According to the calculation plan presented in Section 3.2, three static characteristics of a conceptual brake valve with a differential section were determined. Tab. 3 shows the basic simulation parameters used throughout the study, while Tab. 4 presents the parameters of the local grids used in all configurations - the variables for each of the three cases were the limiting planes of the critical areas.

The use of SolidWorks Flow Simulation software makes it possible to determine the static characteristics of the prototype differential valve solution, with other CFD tools to be used in the course of further work due to the high complexity of the valve's operation and the dynamic processes taking place. The built-in automation tools, including Parametric study and What If Analysis, enabled the valve elements' distance relationships to be changed

smoothly by creating separate simulation configurations. Consideration of each configuration enabled analysis and observation of the MFR and pressure distribution in valve's each chamber.

Tab. 3. Settings of simulation

Parameter	Value
Unit system	SI
Analysis type	Internal
Fluid	Air
Flow type	Laminar and turbulent
Default wall thermal condition	Adiabatic wall
Pressure	$p_0 = 101325 \text{ Pa}$
Temperature	$T_0 = 293.2 \text{ K}$
Turbulence intensity	2%
Turbulence length k	0.0010745 m

Tab. 4. Settings of local mesh

Parameter	Value
Level of refining fluid cells 0-9	3
Level of refining cells at fluid/solid boundary 0-9	3
Number of shells 0-3	2
Maximum equidistant level 0-9	3
Offset distance #1	0.025 mm
Offset distance #2	0.05 mm
Characteristic number of cells across channel	5
Maximum channel refinement level 0-9	3

4.2.1. Static flow characteristics of main supply tract

Following the assumptions of the research plan and the defined boundary conditions of the model, numerical calculations of the main supply tract were carried out over the entire range of operation, and the obtained results are shown in Tab. 5.

Tab. 5. MFR of main supply tract

$h, \text{ mm}$	0	0.1	0.2	0.3	0.4	0.5
MFR, kg/s	0	0.008656	0.018604	0.028012	0.038925	0.050228
$h, \text{ mm}$	0.6	0.7	0.8	0.9	1	1.1
MFR, kg/s	0.059643	0.068209	0.076077	0.086252	0.096242	0.105225
$h, \text{ mm}$	1.2	1.3	1.4	1.5	1.6	1.7
MFR, kg/s	0.112869	0.119811	0.128374	0.137250	0.146309	0.153989
$h, \text{ mm}$	1.8	1.9	2.0			
MFR, kg/s	0.160861	0.168466	0.175830			

The pressure distribution for three different degrees of opening of the main supply tract is shown with a view of the model's computational mesh and in the sensitive area (Fig. 11 – Fig. 13).

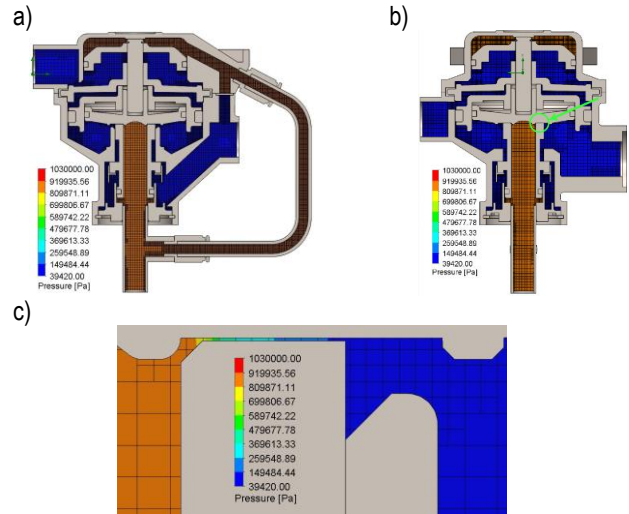


Fig. 11. Pressure distribution for 0.1 mm opening of main supply tract: a – right plane cross-sectional view; b – front plane cross-sectional view; c – detailed view

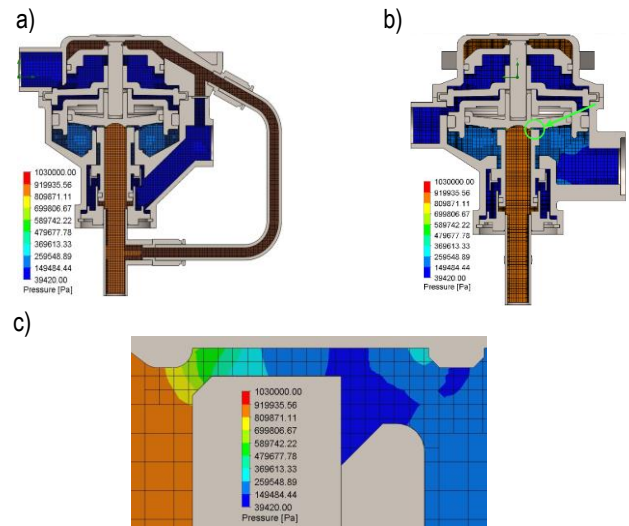


Fig. 12. Pressure distribution for 1.0 mm opening of main supply tract: a – right plane cross-sectional view; b – front plane cross-sectional view; c – detailed view

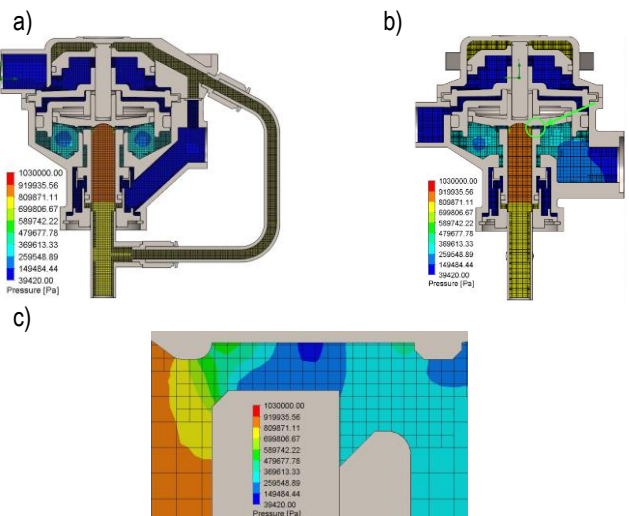


Fig. 13. Pressure distribution for 2.0 mm opening of main supply tract: a – right plane cross-sectional view; b – front cross-sectional view; c – detailed view

Based on the results obtained, the static characteristic of the main supply tract were plotted, which takes on an approximately linear character. In addition, the equation of the regression line shown in Fig. 14 was determined.

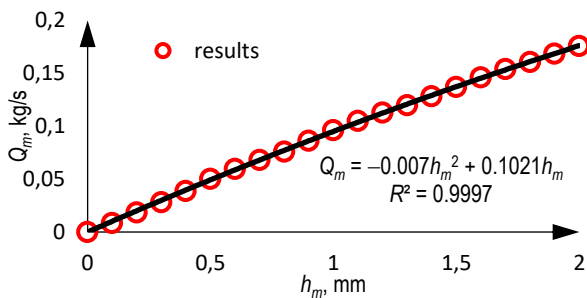


Fig. 14. Static flow characteristic of main supply tract

4.2.2. Static flow characteristics of additional supply tract

Changing the boundary conditions and the direction of the compressed air flow in the model according to the assumptions presented in Section 2.2 will make it possible to determine the static characteristics of the additional supply tract. The results of the numerical calculations carried out for such a configuration are shown in Tab. 6.

Tab. 6. MFR of additional supply tract

$h, \text{ mm}$	0	0.1	0.2	0.3	0.4	0.5
MFR, kg/s	0	0.012464	0.029531	0.049478	0.062523	0.076488
$h, \text{ mm}$	0.6	0.7	0.8	0.9	1	1.1
MFR, kg/s	0.091224	0.107007	0.122079	0.131205	0.138388	0.144086
$h, \text{ mm}$	1.2	1.3	1.4	1.5	1.6	1.7
MFR, kg/s	0.149517	0.153732	0.155939	0.156892	0.157722	0.158217

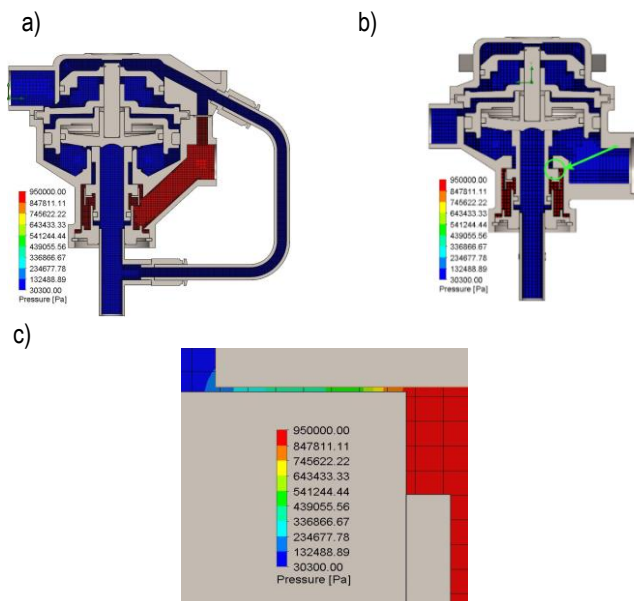


Fig. 15. Pressure distribution for 0.1 mm opening of additional supply tract: a – right plane cross-sectional view; b – front plane cross-sectional view; c – detailed view

The distribution of compressed air pressures for three different degrees of opening of the additional supply tract is shown with a view of the calculation grid in Fig. 15 – Fig. 17.

Based on the obtained MFR values for all degrees of opening of the additional supply tract, the static characteristics was plotted in Fig. 18.

The additional accelerating section of the differential section adopts a degressive character in the range of 1.4-1.7 mm valve opening. It is consistent with authors' previous results obtained in research on the unmodified Visteon valve, so the modifications did not affect the loss of the valve's original performance.

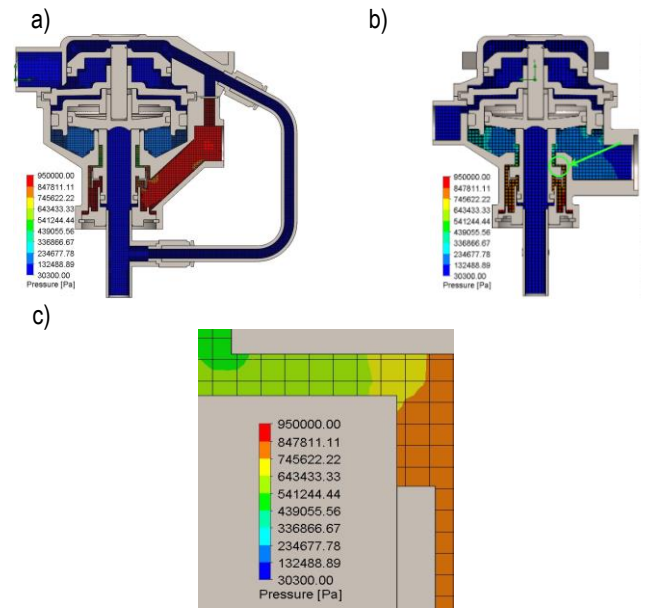


Fig. 16. Pressure distribution for 1.0 mm opening of additional supply tract: a – right plane cross-sectional view; b – front plane cross-sectional view; c – detailed view

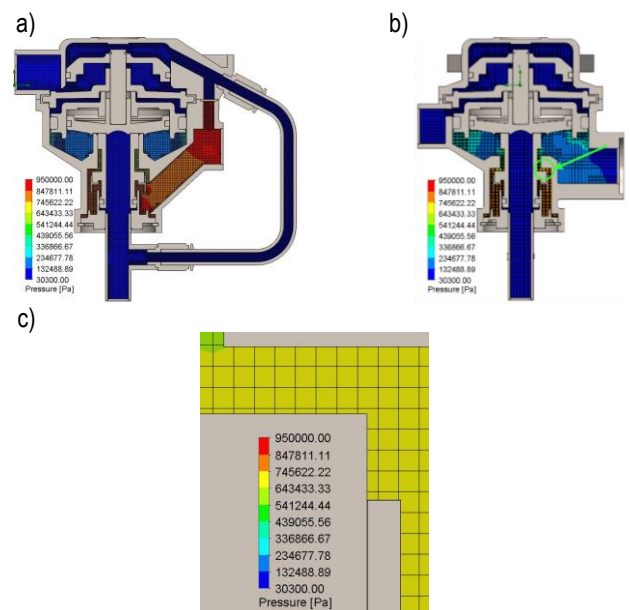


Fig. 17. Pressure distribution for 1.7 mm opening of additional supply tract: a – right plane cross-sectional view; b – front plane cross-sectional view; c – detailed view

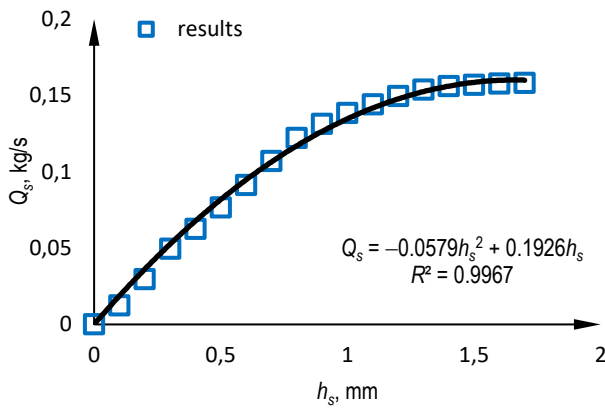


Fig. 18. Static flow characteristics of additional supply tract

4.2.3. Static flow characteristics of differential section

In order to determine the static flow characteristics of the nozzle of the differential section, the model was further simplified by considering only its upper part to reduce calculation time. The nozzle was replaced by a hole in the piston c (Fig. 4) with the diameter assumed in the simulation plan presented in Section 3.2. The results of the numerical calculations carried out for this configuration are shown in Tab. 7.

Tab. 7. MFR of differential tract

<i>h</i> , mm	0.75	1.00	1.25	1.50	1.75
MFR, kg/s	0.000629	0.001243	0.002006	0.002979	0.004078
<i>h</i> , mm	2.00	2.25	2.50	2.75	3.0
MFR, kg/s	0.005387	0.006841	0.008508	0.010271	0.012234

The distribution of compressed air pressures in the differential section for the four nozzle diameters is shown along with views of the calculation grids in Fig. 19.

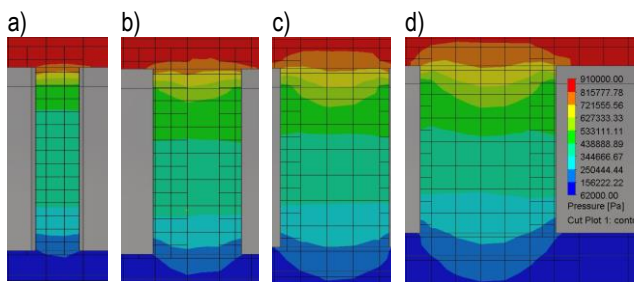


Fig. 19. Pressure distribution for different nozzle diameter: a - 0.75mm; b - 1.50mm; c - 2.25mm; d - 3.0mm

Experimental selection of the diameter of the nozzle connecting the chambers of the differential section, taking into account the geometry of the valve, made it possible to determine the static characteristics of a progressive nature (Fig. 20), with the correct range of nozzle diameters used in the real model to be selected during experimental testing.

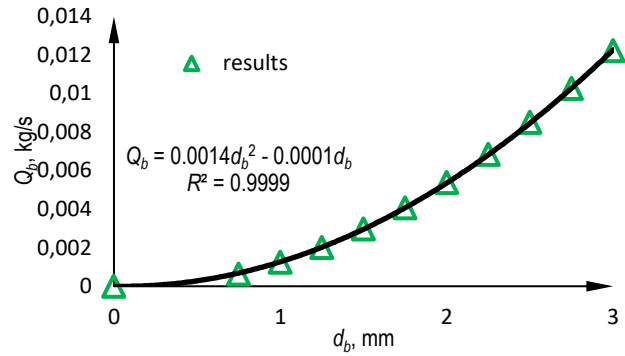


Fig. 20. Bore of the differential section

4.3. Results discussion

Comparing the results of the calculations on a single graph (Fig. 21), there are visible differences in the shapes of the characteristics of the two valve supply tracts. For the purpose of comparisons, the two series of results were matched using the same regression equation based on the least squares method of deviations.

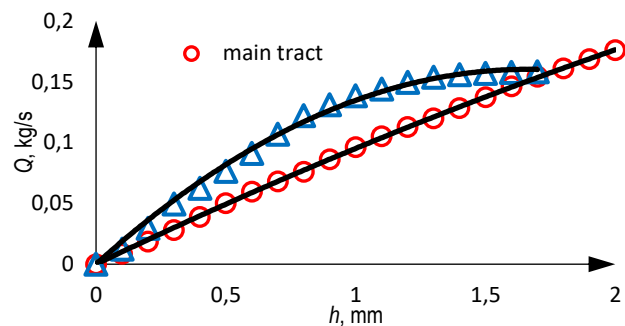


Fig. 21. Main and secondary tract comparison chart

In the main tract, the characteristics are very close to linear, and with a maximum opening of 2 mm the mass flow rate is 0.1758 kg/s. The secondary tract has characteristics with larger increments in the initial opening, while at a maximum opening of 1.7 mm it allows a mass flow rate of 0.1582 kg/s. The final opening range is characterized by a small gradient of increments. Transferring the determined characteristics to the operation of the differential valve, in the case of trailing action, the main-tract characteristics close to linear give the possibility of obtaining proportional action. The intentions of the brake pedal operator are translated into the responses of the braking system. With differential action (emergency braking), the secondary tract guarantees a large increase in mass flow rate even at small openings (at 0.5 mm, the MFR value of the secondary tract is 52.29% higher than the main tract), which promotes acceleration of the braking system. Further down the line, the secondary tract's characteristics stabilize, and at 1.7 mm it approaches the main tract. The differential action of the valve is to accelerate the system in the first phase, which is presented by the secondary line, and in the later stage return to the main tract supply. The important thing here is also the issue of the length of the air supply lines to the main and secondary lines, which are different and have different pressure drop along their length.

An indispensable element affecting the performance of the differential valve is the bore of the differential valve. As can be seen from Fig. 20, changing the diameter of the bore of the piston results in large changes in mass flow rate. Therefore, this diameter and the resulting flow cross-sectional area should be carefully selected for the specific trailer model and even the degree of loading. A large diameter guarantees a rapid return from accelerating to tracking action, while a small diameter delays the process. An inadequate diameter selection can cause trailer jerking in the initial phase of braking under sudden forcing, as well as in the transition from acceleration to tracking. Continuous control of the diameter of the valve that implements the differential action would be required, which is the basis for further work by the authors of the study. As a result, a mechatronic system will be proposed for the permanent correction of the differential action. The characteristics determined in the study are static characteristics applicable to the initial configuration of the pneumatic braking system. Ultimately, it is planned to carry out dynamic calculations in dedicated software for this purpose where it will be possible to evaluate the influence of individual components on the course of the response of the braking system under different types of operator action.

The application of the procedure path presented in the study can find its main application in the configuration of air brake systems, already at the stage of creating new solutions. It can also be useful when retrofitting a design to achieve certain characteristics. Knowledge of the static flow characteristics of flow element determines its performance and functional properties and allows to assess the applicability to a specific usage.

5. CONCLUSIONS

In the study, a series of CFD analyses were carried out to determine the static flow characteristics of the brake valve. The use of global and local computational meshes in the critical flow channels, bounded by the planes of the 3D model geometry of the valve, made it possible to determine the static characteristics of the valve for different tracts of compressed air flow. The limitation of the use of CFD to determine flow parameters is the need to take into account simplifications in the construction of the 3D model and the declaration of constant flow parameters, which may be variable values in the actual operation of the valve, such as temperature. The limitation of the use of SolidWorks Simulation is strictly defined settings of mesh parameters, which cannot be additionally edited and the impact of mesh selection cannot be assessed through indicators such as orthogonal quality and aspect ratio. In further work, the obtained results will be compared with the results obtained in Ansys Fluent and on the constructed test rig. Based on the calculations and analyses, the following conclusions were drawn:

- The static flow characteristics of the main supply tract assume a near linear character. The determined regression equation in the form $Q_m = -0.007 h_m^2 + 0.1021 h_m$ with a coefficient of determination equals $R^2 = 0.9997$ makes it possible to estimate with a high degree of probability the value of the MFR for any degree of opening of the main supply tract. The maximum value of the absolute error was 5.61% with a flow channel height of 0.1 mm.
- The static flow characteristics of the additional supply tract adopted a degressive character, and the determined equation of the regression line $Q_s = -0.0579 h_s^2 + 0.1926 h_s$ and the value of the coefficient of determination equals $R^2 = 0.9967$ testify to a high degree of fit. The estimation of the value of the mass flow rate of the additional supply tract is correct. In the above model configuration, the maximum absolute error value was 8.85% with a flow channel height of 0.2 mm.
- In the last stage of the study, the static characteristics of the differential section were determined at constant volumes of chambers A and B, the variable was the diameter of the hole in the range (0.75..3.0) mm. The characteristics of the differential section took on a progressive character, and the equation of the regression line $Q_b = 0.0014 d_b^2 - 0.0001 d_b$ and the value of the coefficient of determination equals $R^2 = 0.9999$ testify to a very good fit. The maximum value of the absolute error in the case under consideration was 3.90% for a nozzle with a diameter of 1.25 mm.
- Despite the use of local mesh densification, it was noted that the maximum absolute error values occur for channels with heights less than 0.5 mm, while additional local mesh densification would result in significantly longer calculations with little improvement in the obtained result. In addition, in several of the considered model configurations, the SolidWorks Flow Simulation solver reported the occurrence of turbulence, which could disturb the quality of the obtained results, which should be verified using another CFD environment and experimental studies.

Further research work will include the use of dynamic simulations using Ansys Fluent, as well as the construction of a test rig. In the course of further research work, additional parameters affecting the nature of the valve's operation will be taken into account, including the stiffness of the springs used and the diameter of the nozzle using model in Matlab Simulink.

REFERENCES

1. Polichshuk Y, Laptev N, Komarov A, Murzabekov T, Grebenyuk K. Development of agrotechnological requirements for manufacturers of technical tools and agricultural products used in precision farming. *Siberian Herald of Agricultural Science*. 2023;53:98–106.
2. Polischuk Y, Laptev N, Komarov A. The use of automatic and parallel driving systems in agricultural production of the Republic of Kazakhstan and the efficiency of their use. *Agrarian Bulletin of the*. 2020;196:11–9.
3. Ume C. The role of improved market access for small-scale organic farming transition: Implications for food security. *J Clean Prod [Internet]*. 2023;387:135889. Available from: <https://www.science-direct.com/science/article/pii/S0959652623000471>
4. Squalli J, Adamkiewicz G. The spatial distribution of agricultural emissions in the United States: The role of organic farming in mitigating climate change. *J Clean Prod [Internet]*. 2023;414:137678. Available from: <https://www.sciencedirect.com/science/article/pii/S095965262301836X>
5. Sivaranjani S, Rakshit A. Organic Farming in Protecting Water Quality. In: *Organic Farming*. 2019; 1–9.
6. Parizad S, Bera S. The effect of organic farming on water reusability, sustainable ecosystem, and food toxicity. *Environmental Science and Pollution Research*. 2021 Sep;30:1–12.
7. Vdovin S, Bogatyrev M, Nikonorov K, Korotkov P. Reducing the fluid loss in case of depressurization of tractors' hydraulic drive. *Tractors and Agricultural Machinery*. 2023;90:5–12.
8. von Uexküll O, Skerfving S, Doyle R, Braungart M. Antimony in brake pads-a carcinogenic component? *J Clean Prod [Internet]*. 2005;13(1):19–31. Available from: <https://www.sciencedirect.com/science/article/pii/S0959652603001835>
9. Liu Y, Wu S, Chen H, Federici M, Perricone G, Li Y, et al. Brake wear induced PM10 emissions during the world harmonised light-duty vehicle test procedure-brake cycle. *J Clean Prod [Internet]*.

- 2022;361:132278. Available from: <https://www.sciencedirect.com/science/article/pii/S0959652622018820>
10. Commission Regulation (EU) No 1230/2012 of 12 December 2012 implementing Regulation (EC) No 661/2009 of the European Parliament and of the Council with regard to type-approval requirements for masses and dimensions of motor vehicles and their trailers and amending Directive 2007/46/EC of the European Parliament and of the Council.
 11. Koonthalakadu Baby D, Sridhar N, Patil H, Subramanian S. Delay compensated pneumatic brake controller for heavy road vehicle active safety systems. *Proc Inst Mech Eng C J Mech Eng Sci.* 2020;235.
 12. Kazama T. Comparison of power density of transmission elements in hydraulic, pneumatic, and electric drive systems. *Mechanical Engineering Letters.* 2019;5.
 13. Kisiel M, Szpica D, Czaban J. Determination of the flow characteristics of the trailer brake valve using computational fluid mechanics. In: *Proceedings of the 27th International Scientific Conference Mechanika.* 2023.
 14. Subramanian S. Electro-Pneumatic Brakes for Commercial Vehicles – Model Based Analysis for Control and Diagnosis. In: *Schritte in die künftige Mobilität.* 2013; 133–45.
 15. Kisiel M, Szpica D, Czaban J. Effect of differential valve chamber volume on trailer brake system response time. In: *Mechanika 2022 Proceedings of the 26th International Scientific Conference.* Kaunas: Kaunas University of Technology. 2022;32–3.
 16. Basara B, Krajnović S, Pavlovic Z, Ringqvist P. Performance analysis of Partially-Averaged Navier-Stokes method for complex turbulent flows. 2011.
 17. Huang X, Pang B, Chai X, Yin Y. Proposal of a turbulent Prandtl number model for Reynolds-averaged Navier–Stokes approach on the modeling of turbulent heat transfer of low-Prandtl number liquid metal. *Front Energy Res.* 2022;10:928693.
 18. Sang Y, Wang X, Sun W. Analysis of fluid flow through a bidirectional cone throttle valve using computational fluid dynamics. *Australian Journal of Mechanical Engineering.* 2019;19:1–10.
 19. Lee JH, Song X, Park YC, Kang SM. Computational fluid dynamic analysis of flow coefficient for pan check valve. In: *Proceedings of the 9th WSEAS International Conference on Applied Computer and Applied Computational Science.* ACACOS '10. 2010; 157–60.
 20. Zhou XM, Wang ZK, Zhang YF. A simple method for high-precision evaluation of valve flow coefficient by computational fluid dynamics simulation. *Advances in Mechanical Engineering.* 2017;9.
 21. Gabel T, Mitra H, Williams D, Koeck F, Ostilla-Mónico R, Alba K. Incompressible flow through choke valve: An experimental and computational investigation. *J Fluids Struct.* 2022;113:103669.
 22. Garcia S, Iglesias-Rey P, Mora-Meliá D, Martínez-Solano F, Fuentes-Miquel V. Computational Determination of Air Valves Capacity Using CFD Techniques. *Water (Basel).* 2018;10:1433.
 23. Mitra H, Gabel T, Williams D, Koeck F, Ostilla-Mónico R, Alba K. Computational study of compressible flow through choke valve. *J Fluids Struct.* 2022;113.
 24. Hazzi F, Cardona CS, Pairetti C, Venier C. CFD analysis on flow control using a ball valve. *Anales AFA.* 2022;33:21–5.
 25. Gukop N, Kamtu P, Lengs B, Babawuya A, Adegoke A. Effect of Mesh Density on Finite Element Analysis Simulation of a Support Bracket. *FUOYE Journal of Engineering and Technology.* 2021;6.
 26. Lubimyi N, Mihail G, Andrey P, Arseniy S. Methodology for the Selection of Optimal Parameters of the Finite Element Mesh in Composite Materials Calculation. In 2023. p. 66–72.
 27. Pisarciuc C, Dan I, Cioară R. The Influence of Mesh Density on the Results Obtained by Finite Element Analysis of Complex Bodies. *Materials.* 2023;16:2555.
 28. Jurkowski S, Janisz K. Analiza wpływu parametrów siatki obliczeniowej na wynik symulacji przepływomierza. *Autobusy.* 2020;12:129–34.
 29. Kamiński Z, Kulikowski K. Measurement and evaluation of the quality of static characteristics of brake valves for agricultural trailers. *Measurement.* 2017;106:173–8.
 30. Kamiński Z, Kulikowski K. Determination of the functional and service characteristics of the pneumatic system of an agricultural tractor with mechanical brakes using simulation methods. *Eksploatacja i Niezawodność.* 2015;17(3):355–64.
 31. Kamiński Z. Mathematical modelling of the trailer brake control valve for simulation of the air brake system of farm tractors equipped with hydraulically actuated brakes. *Maintenance and Reliability.* 2014;16(4):637–43.
 32. Wu CC, Völker D, Weisbrich S, Neitzel F. The finite volume method in the context of the finite element method. *Mater Today Proc.* 2022;62.
 33. Yang P, Wang X, Li Y. Construction and analysis of the quadratic finite volume methods on tetrahedral meshes. *Sci China Math.* 2023;66:855–86.
 34. Jonuskaite A. Flow simulation with SolidWorks. [Helsinki]: Arcada University of Applied Sciences. 2017.
 35. Sobachkin A, Dumnov G. Numerical Basis of CAD-Embedded CFD. *NAFEMS World Congress.* 2013.
 36. Wang F, di Mare L. Favre-Averaged Nonlinear Harmonic Method for Compressible Periodic Flows. *AIAA Journal.* 2019;57:1–10.
 37. Pavlenko A, Nadrygailo T. On one simulation method of turbulent flows. *Journal of New Technologies in Environmental Science.* 2019;3(4):169–78.

This research was financed through subsidy of the Ministry of Science and Higher Education of Poland for the discipline of mechanical engineering at the Faculty of Mechanical Engineering Białystok University of Technology WZ/WM-IIM/5/2023.

Marcin Kisiel  <https://orcid.org/0000-0002-4576-0447>

Dariusz Szpica  <https://orcid.org/0000-0002-7813-8291>



This work is licensed under the Creative Commons BY-NC-ND 4.0 license.